Phys Chem Minerals (2006) 33:667–676
DOI 10.1007/s00269-006-0115-9

ORIGINAL PAPER

Dauphiné twinning and texture memory in polycrystalline quartz. Part 1: Experimental deformation of novaculite

Hans-Rudolf Wenk · Erik Rybacki · Georg Dresen · Ivan Lonardelli · Nathan Barton · Hermann Franz · Gabriela Gonzalez

Received: 1 April 2006 / Accepted: 29 September 2006 / Published online: 3 November 2006

Abstract Mechanical Dauphiné twinning in quartz has been of long-standing interest, both in single crystals and polycrystalline aggregates. This study investigates texture development in fine-grained quartz rock novaculite with no initial texture using compression experiments conducted in the Paterson gas apparatus to explore the influence of stress and temperature. Texture patterns are measured with time-of-flight neutron diffraction and hard synchrotron X-rays, analyzing diffraction data with the Rietveld method. Similar texture patterns are observed as described previously but the new results establish a profound influence of temperature and document that twinning initiates at stresses less than 50 MPa. Possibilities of using Dauphiné twinning as a paleopiezometer in quartz-bearing rocks are discussed.

Keywords Quartz · Twinning · Texture · Deformation experiments · Synchrotron X-rays

H.-R. Wenk (✉) · I. Lonardelli
Department of Earth and Planetary Science,
University of California, Berkeley, CA 94720, USA
e-mail: wenk@berkeley.edu

E. Rybacki · G. Dresen
GeoForschungsZentrum, Telegrafenberg,
Potsdam 14473, Germany

N. Barton
LLNL, Livermore, CA 94550, USA

H. Franz
DESY, Hamburg 22607, Germany

G. Gonzalez
ESRF, BP220, Grenoble 38043, France

Introduction

Quartz is no doubt one of the most extensively studied minerals with numerous publications discussed in several monographs (e.g., Frondel 1962; Sosman 1965; Heaney et al. 1994). While the composition is simple, the structure displays considerable complexities, particularly that it exists in a right and in a left-handed form, and macroscopic crystals are pervasively twinned.

Since quartz is one of the commonest minerals in the crust, preferred orientation in metamorphic quartzites from tectonic terrains has been of longstanding interest, ever since Schmidt (1925) published the first pole figure. The main texture types have been classified by Sander (1950) and since then quartz pole figures have been used by structural geologists to interpret the deformation history. Most of these studies have based their interpretations on the orientation pattern of *c*-axes of the trigonal mineral that are conventionally measured with the Universal stage. Only recently have diffraction methods been used to obtain the full orientation distribution, particularly the orientation of *a*-axes and of positive and negative rhombs. Few texture investigations discuss the trigonality of many quartz textures and particularly enantiomorphism. Enantiomorphism of quartz in rocks is difficult to quantify (Parkhomenko 1971; Bishop 1981; Ghomshei and Templeton 1989) and is not relevant for the issues addressed in this study. Recently observed systematic trigonality in quartzites has lead us to revisit the issue of Dauphiné twinning in deformed quartzites with experiments and we will report results in three parts: (a) Constrain the stress/temperature influence on twinning with new experiments on fine-grained quartz

rock novaculite using the sensitive Paterson gas deformation apparatus; (b) explore the texture memory effect, when quartz in quartz-bearing rocks is heated above the trigonal–hexagonal phase transformation and cooled again; (c) investigate in situ by neutron diffraction activation of twinning during straining cycles. This report deals with the first part of the study.

Dauphiné twins occur as growth twins as well as mechanical twins (Frondel 1945). Host and twin are geometrically related by a 180° rotation about the *c*-axis. The intergrowth plane in macroscopic crystals is generally irregular. Twinning as well as detwinning can be produced experimentally by applying a shear stress (Fig. 1, Schubnikov and Zinserling 1932; Wooster et al. 1947; Thomas and Wooster 1951; Zinserling 1961). In polycrystalline quartz rocks with an initially random orientation distribution, application of stress can produce a texture by imposing one orientation variant (Tullis 1970; Tullis and Tullis 1972).

However, the role of Dauphiné twins in polycrystalline quartzite has remained enigmatic. They are rarely observed in naturally deformed rocks (e.g., Barber and Wenk 1991; Heidelbach et al. 2000; Lloyd 2000, 2004; Trimby et al. 1998). Since they are produced under relatively low stresses it was suggested that their use as a paleopiezometer is limited and twinning patterns may represent artifacts, unrelated to geological deformation processes (Tullis 1980). But recent studies indicate that regular trigonal orientation distributions have formed during tectonic deformation (Pehl and Wenk 2005) as well as by shock deformation during meteorite impact (Trepmann and Spray 2005; Wenk et al. 2005). This revived interest to better quantify the influence of stress and temperature on the activity of twinning.

Deformation experiments

Samples of novaculite, a fine-grained dense quartz rock from Arkansas, were used as material. Novaculite is very homogeneous, with grain size of about 10 μm (Fig. 2), has no initial preferred orientation and minimal porosity. Naturally occurring novaculite is largely undeformed with no apparent strain or stress features. It was previously used by Tullis and Tullis (1972) to investigate Dauphiné twinning. In that study a Griggs solid pressure medium deformation apparatus was used, where stress is poorly defined and large temperature gradients exist. Two parameters were of prime interest in this study, compressive stress and temperature. They were established previously as influential (Thomas and Wooster 1951; Tullis and Tullis 1972). Confining pressure appears less important with experiments at ambient pressure (Thomas and Wooster 1951) providing similar results as experiments at 400 MPa (Tullis and Tullis 1972). Also the duration of applying stress does not seem to influence texture patterns. Already Schubnikov and Zinserling (1932) showed that twinning was activated instantaneously and this was later confirmed (Wooster and Wooster 1946).

Experiments were conducted in a high-precision Paterson-type gas deformation apparatus (Paterson 1970). The apparatus is equipped with a gas-pressure vessel with internal load cell and multi-zone furnace. For experiments we used cylindrical samples of 20 mm

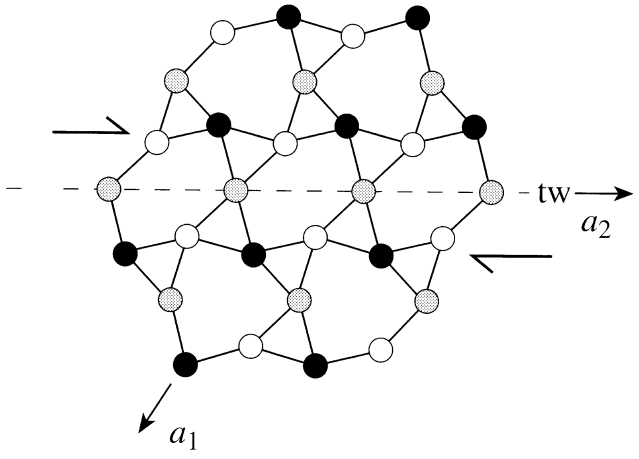

Fig. 1 Model for the structure of a mechanical Dauphiné twin produced by shear, [0001] projection (Schubnikov and Zinserling 1932). Twin plane (*tw*) and sense of shear are indicated. Only Si atoms are shown with *gray shades* different *z*-coordinates

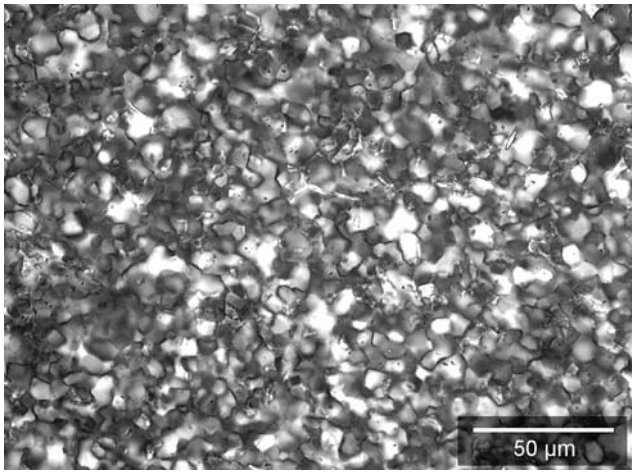

Fig. 2 Microstructure of novaculite used in this study. Crossed polars

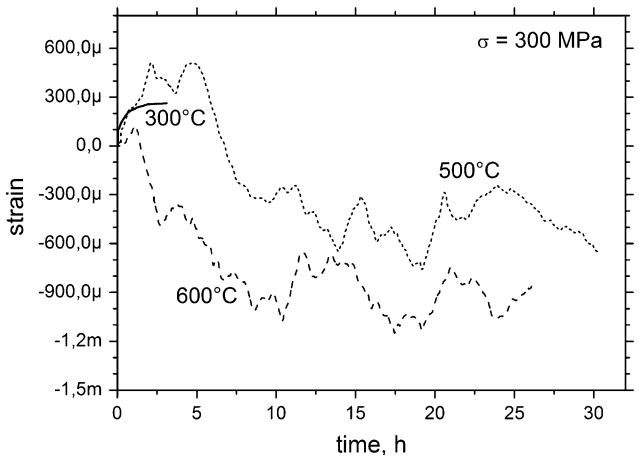

Fig. 3 Plot of microstrain as function of time for samples N2-1 (300°C), N2-9 (500°C), N2-11 (600°C)

length and 10 mm diameter, jacketed by a thin iron-sleeve to prevent intrusion of the argon pressure medium. Axial loading is applied by an electro-mechanical actuator. Accuracy of axial stress is <3% and temperature is constant within 3°C.

Experiments proceeded as follows. First confining pressure was increased to 260–280 MPa, then temperature was raised to the desired value at 20°C/min. This increased the confining pressure to the planned value of 300 MPa. This confining pressure is similar to that applied by Tullis and Tullis (1972) and is applied to keep the material from fracturing under compressive stress. Now the sample was elastically loaded to the maximum value at a rate of 5 kN/min and kept for time t. Stress was kept constant within 2% over the duration of the experiment. There is slight shortening during the first few hours (<1,000 microstrain) that in part is due to relaxation of the apparatus, rather than sample deformation (Fig. 3). In any case sample deformation is minimal. At the end temperature was decreased with a rate of 30–40°C/min, maintaining axial load. At 100–200°C load was decreased and confining pressure reduced. Table 1 summarizes experimental conditions. Most of the samples were maintained under load for 31 h. Only for 300°C experiments one 31-h and three 3 h experiments were conducted.

Texture analysis

Mechanical twinning results in a crystal reorientation and in a polycrystal with a large number of crystallites there are changes in the orientation distribution (OD or texture). If the material has initially a random OD, then mechanical twinning under stress will produce a texture pattern, with some crystals twinning and others not. Changes in the OD are expressed in diffraction patterns, particularly intensity variations along Debye rings. We are using diffraction methods to determine the texture. Measurements were done both with neutron and synchrotron X-ray diffraction. The advantage of neutrons is a good average over a large sample. Synchrotron X-rays probe a smaller volume but data acquisition is very fast.

For neutron diffraction the sample cylinders could be used directly for the measurements. The time-of-flight diffractometer HIPPO at the Los Alamos Neutron Science Center was employed. HIPPO is optimized for texture measurements and experimental details are given by Wenk et al. (2003). A collimated beam of thermal neutrons (wavelengths 0.2–6 Å), 1–2 cm in diameter, enters the HIPPO diffractometer with a 9 m distance between spallation source and sample. Neutrons are diffracted on the sample and the time of flight (TOF) of the diffracted neutrons is measured by an array of 30 detector panels arranged on three banks with different 2θ angles (40°, 90° and 150°). Each detector records diffraction spectra from

Table 1 Experimental conditions (all samples at 300 MPa confining pressure) and texture information

Sample	*T* (°C)	Stress (MPa)	Time (h)	Texture facility	ODF max/min (m.r.d.)
N2-1	300	300	3	HASY, HIPPO	1.06–0.93, irregular
N2-2	300	150	3		Not measured
N2-3	300	450	3	HASY, HIPPO	1.07-0.94, irregular
N2-5	500	600	31	HASY	1.77–0.33
N2-6	500	600	31	HASY	1.77–0.30
N2-7	300	600	31	HASY	1.11–0.89, weak texture
N2-8	500	450	31	HASY	1.74–0.28
N2-9	500	300	31	ESRF, HIPPO	1.33–0.61
N2-10	500	150	30.5	ESRF, HIPPO	1.04–0.95, weak texture
N2-11	600	300	30.5	ESRF, HIPPO	1.96–0.07
N2-12	600	150	30.5	ESRF	1.62–0.27
N2-13	600	50	30.5	ESRF	1.10–0.86

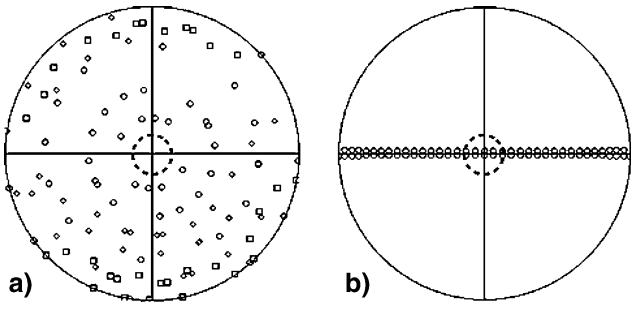

Fig. 4 Pole figure coverage **a** with HIPPO neutron diffraction data (*circles* are 150° detectors, *squares* 90° and *diamonds* 40°) and **b** with a single synchrotron X-ray diffraction image. Compression direction is in the center (*dashed ring*)

differently oriented crystals and the intensity variations of diffraction peaks document differences in crystallite orientation. The cylindrical samples were mounted on an aluminium rod and inserted into an automatic sample changer. The orientation coverage is improved by rotating the cylindrical sample in four increments about the vertical axis (0°, 45°, 67.5°, 90°), resulting in $4 \times 30 = 120$ orientations (Fig. 4a). TOF diffraction spectra were recorded for approximately 5 min, amounting to a total data acquisition time of 20 min per sample.

For synchrotron X-rays 1 mm thick slabs through the central portion of the cylinder were prepared. Experiments were done with hard monochromatic X-rays at beamline PETRA2 at HASYLAB 6 of the German Synchrotron facility (DESY) in Hamburg and at beamline ID-15B of the European Synchrotron Radiation Facility (ESRF) in Grenoble. The sample slab was mounted on a metal rod and analyzed in transmission. The geometry of the experiment has been described by Wenk and Grigull (2003). It relies on intensity variations along Debye rings. Pole figure coverage along a Debye ring is illustrated in Fig. 4b. The compression direction is indicated. In the initial analysis of diffraction images no symmetry was imposed but the final analysis relied on axial symmetry about the compression direction.

At DESY a monochromatic beam of wavelength of 0.1848 Å, 1×2 mm in size, was used. Diffraction images were collected with a MAR345 image plate detector mounted at 129.75 cm from the sample ($2{,}300 \times 2{,}300$ pixels). Counting times for individual images were 180 s. At ESRF wavelength was 0.13965 Å and the beam size 0.5×0.5 mm. A MAR345 image plate was mounted at 82.40 cm. Exposures were for 10 s, translating the sample 2 mm along the cylinder axis for better averaging. After data collection images were corrected in FIT2D (Hammersley 1998) for distortion and tilt, relying on a LaB_6 standard. Corrected images were exported from FIT2D in 16-bit tiff format for further processing.

Both neutron diffraction spectra and synchrotron X-ray images were analyzed for texture with the Rietveld code MAUD (Material Analysis Using Diffraction) (Lutterotti et al. 1999). This program was recently modified to accept synchrotron diffraction images (Lonardelli et al. 2005). In the case of neutrons, 120 experimental spectra in GSAS format (Larson and Von Dreele 2004) were imported. For X-rays, tiff images with 16 bit dynamic range are entered, using an image manager where it is possible to set the correct parameters (sample/detector distance, ranges for integration, center coordinates, number of spectra etc.). In this study 72 spectra were obtained by integrating over azimuthal sectors of 5°.

Dauphiné twinning, a twofold rotation about the *c*-axis, is only ''visible'' with general reflections of type (*hkil*) and particularly rhombohedral reflections (*h*0–*hl*) and invisible with (0001), $(10\bar{1}0)$, $(11\bar{2}0)$ and $(hh\bar{2}hl)$ type reflections. Furthermore reflections for positive rhombs (e.g., $10\bar{1}1$) and negative rhombs (e.g., $01\bar{1}1$) are exactly at the same *d* spacing and thus overlap in the diffraction pattern. Texture is only visible in the diffraction pattern because structure factors for positive and negative rhombs are different for trigonal quartz (Baker and Wenk 1972, Table 2 gives scattering factor contributions to the overlapped peak for neutrons and X-rays). The relative contributions are quite different for neutrons and X-rays and in some cases even reversed. Figure 5a shows a stack of neutron spectra (90° detector) and Fig. 5b corresponding X-ray spectra integrated from diffraction images. Some texture is visible for lines $(10\bar{1}2)$, $(20\bar{2}1)$, and (02–22) as intensity variations relative to the angle with the compression direction. Variations are larger for X-rays where data span the whole range from parallel to perpendicular to the compression direction than for neutrons where all detectors are at high angles to the compression direction. There are no such systematic variations for lines $(11\bar{2}0)$ etc. Note that the line $(20\bar{2}0)$ at $d = 2.13$ Å is very weak for neutrons because of a weak structure factor. MAUD uses these intensity variations to extract the orientation distribution (OD). The present analysis relies on the tomographic method EWIMV, a variation of WIMV (Matthies and Vinel 1982). OD cells were chosen as 10°. From the OD pole figures and inverse pole figures were recalculated and are used for representation.

Figure 6a displays $(10\bar{1}1)$ and $(01\bar{1}1)$ pole figures recalculated from the ODF for sample N2-11 measured by neutron diffraction. The compression direction is in

Table 2 Intensity contributions to overlapped rhombohedral reflections for neutrons and X-rays (in %)

	d (Å)	Neutrons	X-rays
1011	3.347	72	70
0111	3.347	28	30
1012	2.283	91	14
0112	2.283	09	86
2011	1.982	11	31
0211	1.982	89	69
$20\bar{2}2$	1.674	86	81
$02\bar{2}2$	1.674	14	19
$10\bar{1}3$	1.661	65	99
$01\bar{1}3$	1.661	35	01
21–31	1.543	85	55
12–31	1.543	15	45

the center. The pole figures display overall axial symmetry, consistent with the deformation conditions. Pole figures of positive rhombs $(10\bar{1}1)$ display a maximum in the compression direction (center) and for negative rhombs $(01\bar{1}1)$ a minimum.

The same sample was also measured with synchrotron X-rays and the Rietveld analysis was performed with a single image, using procedures described by Ischia et al. (2005). In this case the pole figure coverage is minimal (Fig. 4b) but nevertheless useful information can be obtained. Figure 6b shows the same pole figures as for neutrons and there is a close resemblance. Axial symmetry is less perfect which is an artifact of the highly incomplete coverage. For neutrons low pole density regions have higher values than for X-rays. This could be an artifact of the coverage. For X-rays there are data from parallel to perpendicular to the compression direction. For neutrons only low-resolution 40° detectors are close to the compression direction (Fig. 4a). For this reason we prefer X-ray data for this particular study. In hindsight for neutrons the sample should have been mounted with the compression direction perpendicular to the rotation axis. Also, for neutrons axial symmetry is not perfect due to the coverage biased by detector geometry. But overall results document that both neutron and X-ray diffraction produce similar results for these relatively weak textures. Having established axial symmetry of the texture, in all successive analyses this symmetry was imposed, when calculating the orientation distribution and results are displayed in inverse pole figures of the compression direction.

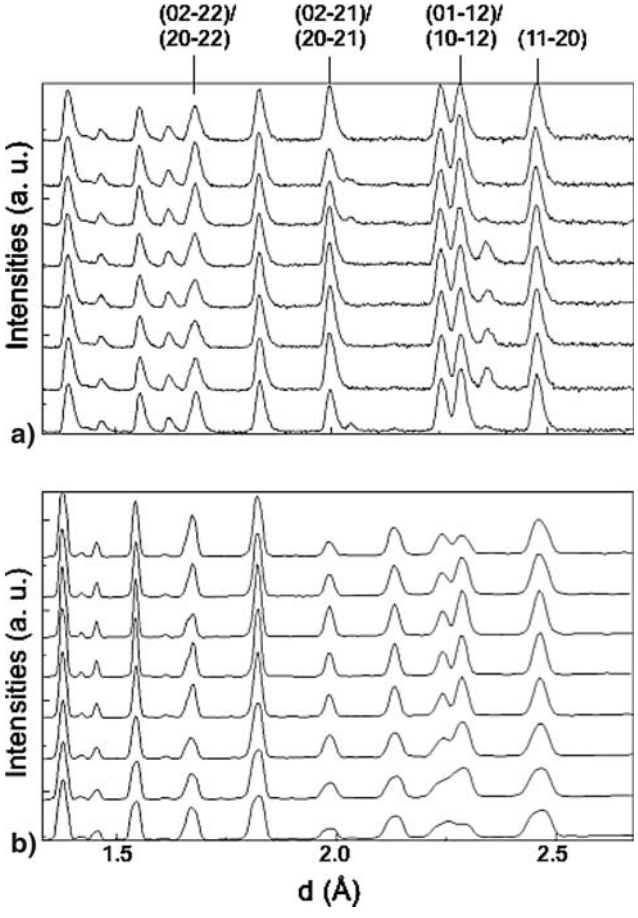

Fig. 5 **a** Sample N2-11. Stack of diffraction patterns of **a** neutron diffraction data, 90° detectors and **b** X-ray diffraction image. Ordinate is intensity in arbitrary units, abscissa is in *d*-spacing. Texture is visible in intensity variations of rhombohedral lattice planes

Results

Inverse pole figures are shown in Figs. 7 and 8. First we document reproducibility by deforming two samples at identical conditions (N2-5 and N2-6, Fig. 7a, b). The agreement is excellent, both in terms of pattern as well as maximal and minimal values, confirming both the validity of experiments as well as analytical data reduction. The comparison of inverse pole figures for neutron diffraction and X-ray diffraction on the same sample illustrates a similar pattern but differences in maxima and particularly minima as already commented on above (N2-11 with neutrons at LANSCE and X-rays at ESRF, Fig. 7c, d). We attribute the differences to the special coverage for neutrons and we are relying on X-rays for all other results.

Figure 8 shows inverse pole figures for all samples for different temperatures and stress and minima and maxima are also summarized in Table 1. Note that in these figures pole densities are contoured with two different linear scales, 0.2–1.8 multiples of a random distribution (m.r.d.) for stronger textures and

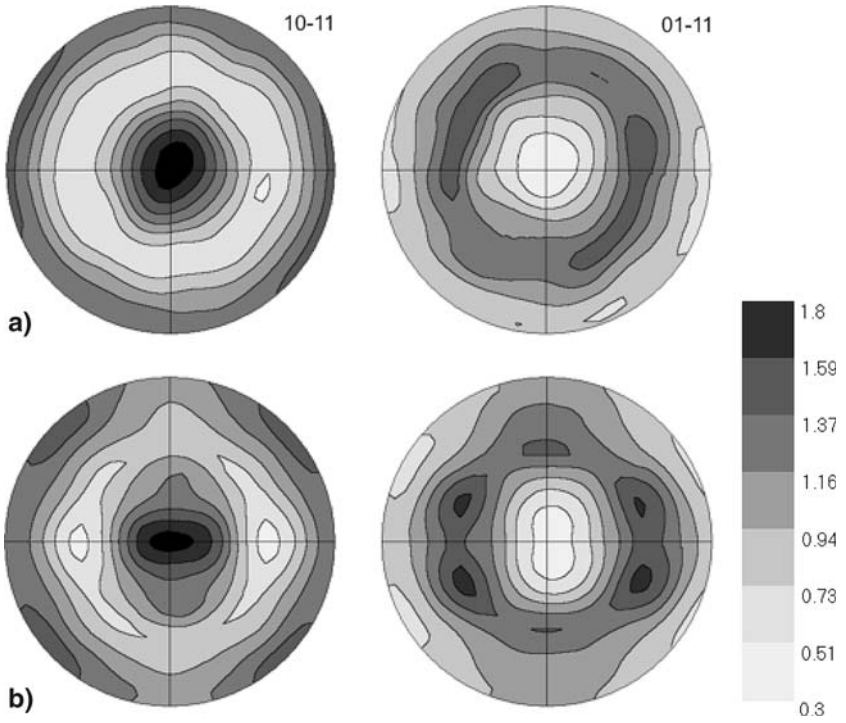

Fig. 6 Pole figures for sample N2-11 without imposing sample symmetry. **a** Neutron diffraction, **b** synchrotron X-rays. Compression direction is in the center. Equal area projection, linear contours

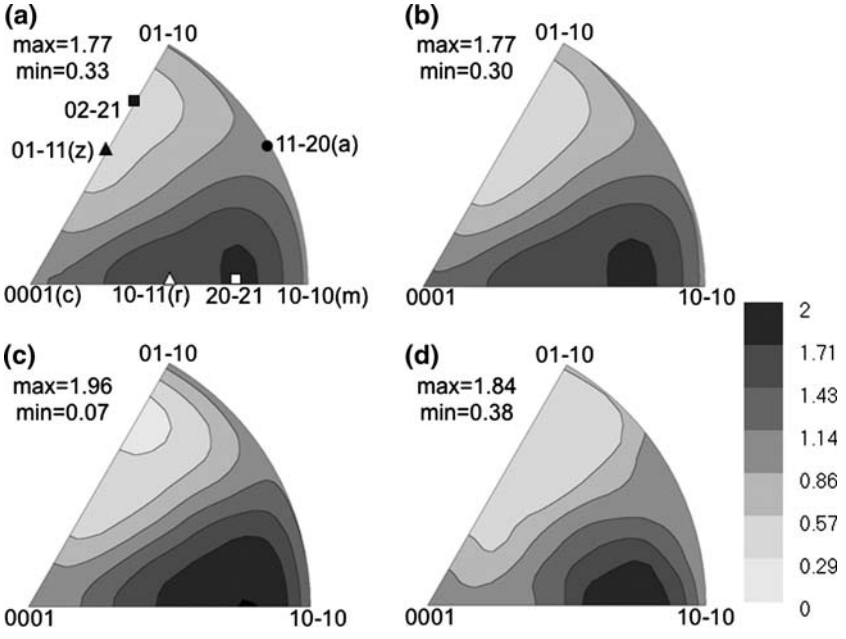

Fig. 7 Inverse pole figures of the compression direction establishing reproducibility. **a**, **b** Two samples (N2-5, N2-6) deformed at identical conditions and measured with synchrotron X-rays. **c**, **d** Same sample (N2-11) measured with synchrotron X-rays and neutrons, respectively. Axial symmetry is imposed. Equal area projection, linear contours, m.r.d. units

0.8–1.2 m.r.d. for weak textures. Low temperature experiments (300°C) have no significant texture or best at 600 MPa a very weak texture develops. The most difficult part is to establish a random or very weak orientation pattern. All other samples do display texture with low pole density regions for negative rhombs and high-density regions for positive rhombs. At 500°C a weak texture is documented at 150 MPa, at 600°C even at 50 MPa positive rhombs have higher pole densities.

Discussion

The preferred orientation patterns that are observed are similar to those reported by Tullis and Tullis (1972)

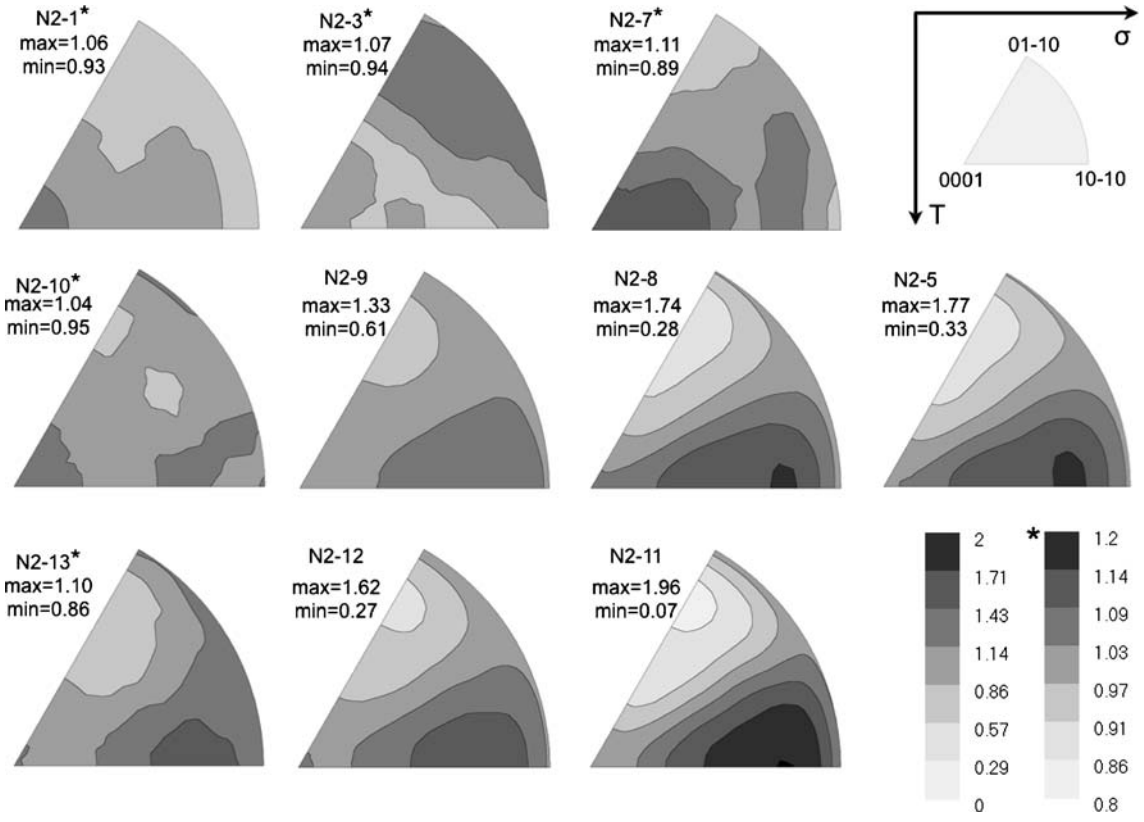

Fig. 8 Inverse pole figures documenting variation of texture with temperature and differential stress. *Top row* is 300°C, *center* 500°C and *bottom row* 600°C. For stresses see Table 1. Axial symmetry is imposed for obtaining the orientation distribution. Two scales are used for contouring. Scale 2 is marked with *asterisk*. Linear contours

with a solid pressure medium piston-cylinder apparatus. There is a depletion of negative rhombs and an anti-symmetrical increase in positive rhombs. Since the earlier study, deformation experiments have been refined and methods of texture analysis, both experimental and data processing, have much improved. For example in Tullis and Tullis (1972) many inverse pole figures show regions with negative pole densities, as well as concentrations above 2 m.r.d., both of which are not possible. In the new study the highest pole densities are 1.96 m.r.d. and the minimum is 0.07 m.r.d. Except for one old experiment (GB-412 at 300°C, 220 MPa) all experiments with the Griggs solid pressure medium apparatus applied much higher stresses, most above 1 GPa. The GB-412 sample with a texture maximum of 1.55 m.r.d. is somewhat of an oddity because at 300°C we observed no texture up to 600 MPa and at that stress the maximum is only 1.11 m.r.d. We have no explanation except the caveat that stresses in a Griggs apparatus are not very well defined.

In all inverse pole figures the $a = 11\bar{2}0 - c = 0001$ plane is more or less a pseudo mirror plane. Maxima and minima are centered in the vicinity of $20\bar{2}1$ and $02\bar{2}1$. Twinning reduces pole densities along negative rhombs and increases positive rhombs. If the initial texture is random and twinning is the only mechanism, then depleted and augmented regions should be exactly antisymmetrical, as observed. If twinning is complete (i.e., all grains twin) then pole densities for negative rhombs are reduced to zero and those for positive rhombs double (2 m.r.d.). There can be no pole densities larger than 2.0 m.r.d.

Obviously there is an orientation effect on the efficiency of twinning. Orientations with the $02\bar{2}1$ pole parallel to the compression direction twin most easily and twinning is almost complete with pole densities close to zero at $02\bar{2}1$ and close to 2.0 at $20\bar{2}1$, e.g., in the case of N2-11. Twinning activity decreases greatly with angular distance from these orientations.

Thomas and Wooster (1951) were the first to attribute mechanical twinning to maximizing elastic strain and Klassen-Neklyudova (1964), McLellan (1978) and Markgraaf (1986) used a thermodynamic approach to calculate the energy change on twinning. The single crystal Young's modulus, calculated from elastic constants is strikingly similar to the texture patterns

(Figs. 9a, 10). The difference in Young's modulus for negative minus positive forms (Fig. 9b) may be used to estimate the driving force for Dauphiné twinning and orientations away from $02\bar{2}1$ are less likely to twin. With temperature quartz becomes weaker (Ohno 1995; Ohno et al. 2006) but the difference between directions that are related by Dauphiné twinning barely changes with temperature (Fig. 9b). Pehl and Wenk (2005) have used this difference, combined with a random number generator, to simulate twinning in polycrystalline aggregates and obtained a good empirical model for compressive twinning. The experiments show evidence that twinning increases with applied stress but saturates long before it is complete. Most interesting are experiments at 500°C that document a gradual increase in texture above 150 MPa and saturation at 450 MPa. Increasing stress to 600 MPa does not activate twinning in less favorably oriented grains (Fig. 8, N2-8 and N2-5).

The new experiments document a profound influence of temperature on the activation of twinning that is highlighted in Fig. 10. At 300°C no significant twinning is activated. At 600 MPa a very slight difference between positive and negative rhombs develops. By contrast, at 600°C twinning initiates below 50 MPa and saturates at 300 MPa. This is close to the phase transformation (640°C at 300 MPa confining pressure, van Groos and Heege 1973).

To at least some degree, the behavior may be rationalized in terms of twinning kinetics based on activation energy. In this context, probability of twinning becomes a mass fraction rate of twinning, with the rate depending on the driving force, temperature, and activation energy. The barrier height for twinning decreases with temperature (Smirnov and Mirgorodsky 1997), motivating a temperature-dependent activation energy. A decrease in activation energy as the α–β transformation temperature is approached is consistent with experimental observations of extensive small scale twinning near the transformation temperature (Sorrell et al. 1974; Van Tendeloo et al. 1976; Barber and Wenk 1991; Heaney and Veblen 1991). Effects from the mechanical part of the driving force are complicated by the lack of a change in lattice strain at zero stress. That is, twinning at zero stress would not produce strain in quartz. Twinning under stress does, however, produce strain due to the above mentioned elastic anisotropy. Barton et al. (2005) derive a mechanical driving force that includes the effects of elastic anisotropy for general states of stress. Therefore, the leading term in the mechanical contribution to the driving force is quadratic in stress instead of being linear in stress. This quadratic dependence may complicate the grain interaction effects in a polycrystal and could bear on the saturation of twinning observed at 500°C.

In this investigation we have kept variables to a minimum by performing all experiments on the same novaculite samples at the same confining pressure. It is likely that other parameters may influence activation of mechanical twinning such as grain size and OH content of quartz. This will be the subject of future studies. Also, in the experiments described here the same path was followed: application of confining pressure, increase in temperature, then increase in compressive stress. At the maximum stress reducing temperature to ambient, then lowering stress and

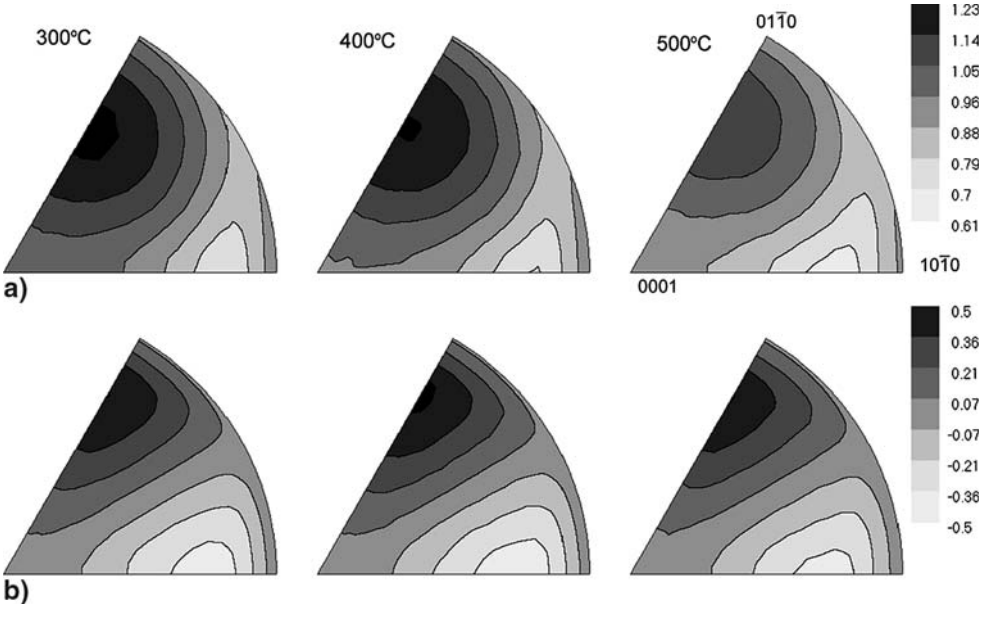

Fig. 9 **a** Single crystal Young's moduli at different temperatures (Ohno 1995; Ohno et al. 2006). **b** difference of Young's moduli for positive and negative forms (in GPa/100, linear contours)

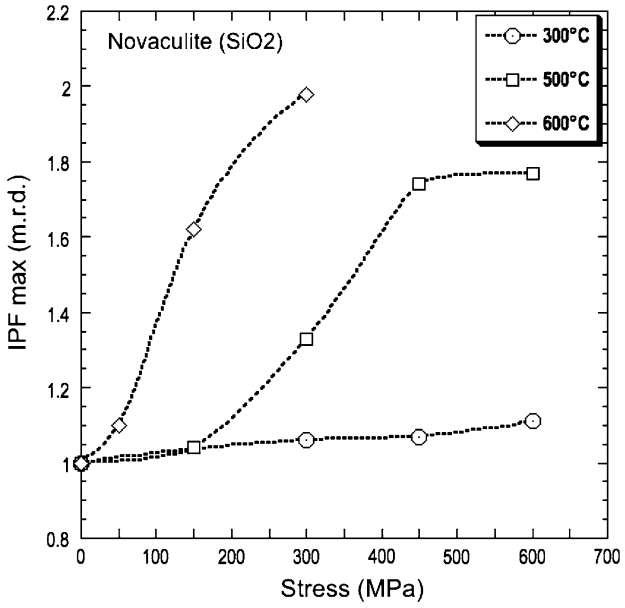

Fig. 10 Maximum pole density in inverse pole figure (*IPF*) versus stress for different temperatures, illustrating approximate initiation and saturation of mechanical twinning in novaculite

finally confining pressure. Conceivably, if differential stress were lowered at temperature, some twinning might be reversed under the influence of residual stresses imposed by neighboring grains and future experiments should be conducted in situ at stress and temperature. The currently obtained texture patterns may not reveal the maximum twinning activity during the experiment.

Also, we did not address the influence of time. Most experiments were done over about 30 h. Only at 300 C we compared short times (3 h) and long times (31 h) and did not find an appreciable difference. It is conceivable that at intermediate temperatures time may play a role and we will address this with future in situ experiments. At least for single crystals it appears that twinning is almost instantaneous (Schubnikov and Zinserling 1932; Wooster and Wooster 1946).

The present study documents a low threshold for mechanical twinning in polycrystalline quartz. Particularly at higher temperature twinning may initiate at less than 50 MPa which is within tectonic stresses, at least local concentrations in shear zones and faults. Thus Dauphiné twinning may well be useful as a paleopiezometer to estimate stress fields, as well as stresses and systematic investigations of quartz-bearing rocks are warranted, in a similar approach as used by Pehl and Wenk's (2005) study of mylonites.

Acknowledgments We are appreciative to M. Naumann, S. Gehrmann and K. Peach for help with deformation experiments and sample preparation. Jan Tullis provided some of the samples and inspiring discussions. Comments from a reviewer were most helpful. Texture measurements were performed at synchrotron beamlines PETRA2 at HASYLAB 6 (DESY) and ID 15B of ESRF. Some samples were also measured by neutron diffraction with HIPPO at LANSCE with the help of Sven Vogel. HRW is grateful for hospitality at the GeoForschungsZentrum Potsdam during a sabbatical leave. The work of NB was performed under the auspices of the U.S. Department of Energy by University of California, Lawrence Livermore National Laboratory under Contract W-7405-Eng-48 (UCRL-JRNL-220357). Research was supported by NSF (EAR 0337006) and DOE (DE-FG02-05ER15637).

References

Baker DW, Wenk H-R (1972) Preferred orientation in a low symmetry quartz mylonite. J Geol 80:81–105

Barber DJ, Wenk H-R (1991) Dauphiné twinning in deformed quartzites: implications of an in situ TEM study of the α–β phase transformation. Phys Chem Miner 17:492–502

Barton NR, Benson DJ, Becker R (2005) Crystal level continuum modelling of phase transformations: the $\alpha \leftrightarrow \varepsilon$ transformation in iron. Model Simul Mater Sci Eng 13:707–731

Bishop JR (1981) Piezoelectric effects in quartz-rich rocks. Tectonophysics 77:297–321

Frondel C (1945) Secondary Dauphiné twinning in quartz. Am Mineral 30:447–461

Frondel C (1962) The system of mineralogy, 7th edn, vol 3. Wiley, New York

Ghomshei MM, Templeton TL (1989) Piezoelectric and *a*-axis fabric along a quartz vein. Phys Earth Planet Int 55:374–386

Hammersley AP (1998) Fit2D: V99.129 reference manual, version 3.1. Internal Report ESRF-98-HA01

Heaney PJ, Veblen DR (1991) Observation and kinetic analysis of a memory effect at the α–β quartz transition. Am Mineral 76:1459–1466

Heaney PJ, Prewitt CT, Gibbs GV (1994) Silica. Physical behavior, geochemistry and materials applications. Rev Mineral Min Soc Am 29:606

Heidelbach F, Kunze K, Wenk H-R (2000) Texture analysis of a recrystallized quartzite using electron diffraction in the scanning electron microscope. J Struct Geol 22:91–104

Ischia G, Wenk H-R, Lutterotti L, Berberich F (2005) Quantitative Rietveld texture analysis of zirconium from single synchrotron diffraction images. J Appl Cryst 38:377–380

Klassen-Neklyudova MV (1964) Mechanical twinning of crystals (translated from Russian by JES Bradley). Consultants Bureau, New York, p 213

Larson AC, Von Dreele RB (2004) General structure analysis system (GSAS). Los Alamos National Laboratory Report LAUR 86-748

Lloyd GE (2000) Grain boundary contrast effects during faulting of quartzite: an SEM/EBSD analysis. J Struct Geol 22:1675–1693

Lloyd GE (2004) Microsturctural evolution in a mylonitic quartz simple shear zone: the significant roles of dauphine twinning and misorientation. In: Alsop GI et al (eds) Transports and flow processes in shear zones. Geological Society of London, Special Publication, vol 224, pp 39–61

Lonardelli I, Wenk H-R, Lutterotti L, Goodwin M (2005) Texture analysis from synchrotron diffraction images with the Rietveld method: dinosaur tendon and salmon scale. J Synchrotron Rad 12:354–360

Lutterotti L, Matthies S, Wenk H-R (1999) MAUD: a friendly Java program for materials analysis using diffraction. Int Union Crystallogr Comm Powder Diffr Newsl 21:14–15

Markgraaf J (1986) Elastic behavior of quartz during stress-induced Dauphiné twinning. Phys Chem Miner 13:102–112

Matthies S, Vinel GW (1982) On the reproduction of the orientation distribution function of textured samples from reduced pole figures using the concept of conditional ghost correction. Physica Status Solidi B 112:K111–K114

McLellan AG (1978) The thermodynamic theory of the growth of Dauphiné twinning in quartz under stress. J Phys C 11:4665–4679

Ohno I (1995) Temperature variation of elastic properties of α-quartz up to the α–β transition. J Phys Earth 43:157–169

Ohno I, Harada K, Yoshitomi C (2006) Temperature variation of elastic constants of quartz across the α–β transition. Phys Chem Miner 33:1–9

Parkhomenko EI (1971) Electrification phenomena in rocks. (Translation by GV Keller). Plenum Press, New York, 285 pp

Paterson MS (1970) A high-pressure, high-temperature apparatus for rock deformation. Int J Rock Mech Mining Sci Geomech Abstr 7:517–526

Pehl J, Wenk H-R (2005) Evidence for regional Dauphiné twinning in quartz from the Santa Rosa mylonite zone in Southern California. A neutron diffraction study. J Struct Geol 27:1741–1749

Sander B (1950) Einführung in die Gefügekunde der geologischen Körper. Springer, Vienna

Schmidt W (1925) Gefügestatistik. Tschermaks Mineral Petrog Mitt 38:392–423

Schubnikov A, Zinserling K (1932) Ueber die Schlag- und Druckfiguren und ueber die mechanische Quartzzwillinge. Z Kristallogr 83:243–264

Smirnov MB, Mirgorodsky AP (1997) Lattice-dynamical study of the α–β phase transition of quartz: soft-mode behavior and elastic anomalies. Phys Rev Lett 78:2413–2416

Sorrell AC, Anderson HU, Ackermann RJ (1974) Thermal expansion and the high-low transformation in quartz. II. Dilatometric studies. J Appl Cryst 7:468–473

Sosman RB (1965) The phases of silica. Rutgers University Press, New Brunswick, 388 pp

Thomas LA, Wooster WA (1951) Piezocrescence—the growth of Dauphiné twinning in quartz under stress. Proc R Soc Lond A 208:43–62

Trepmann CA, Spray JG (2005) Planar microstructures and Dauphiné twins in shocked quartz from the Charlevoix impact structure, Canada. Geol Soc Am Spec Pap 384:315–328

Trimby PW, Prior DJ, Wheeler J (1998) Grain boundary hierarchy development in a quartz mylonite. J Struct Geol 20:917–935

Tullis J (1970) Quartz: preferred orientation in rocks produced by Dauphiné twinning. Science 168:1342–1344

Tullis TE (1980) The use of mechanical twinning in minerals as a measure of shear stress magnitudes. J Geophys Res 85:6263–6268

Tullis J, Tullis TE (1972) Preferred orientation produced by mechanical Dauphiné twinning. Thermodynamics and axial experiments. Am Geophys U Monogr 16:67–82

Van Groos AFK, Heege JPT (1973) The high-low quartz transition up to 10 kb pressure. J Geol 81:717–724

Van Tendeloo G, Van Landuyt J, Amelickx S (1976) The α–β phase transition in quartz and $AlPO_4$ as studied by electron microscopy and diffraction. Physica Status Solidi A 33:723–735

Wenk H-R, Grigull S (2003) Synchrotron texture analysis with area detectors. J Appl Cryst 36:1040–1049

Wenk H-R, Lutterotti L, Vogel S (2003) Texture analysis with the new HIPPO TOF diffractometer. Nuclear Instrum Methods A515:575–588

Wenk H-R, Lonardelli I, Vogel SC, Tullis J (2005) Dauphiné twinning as evidence for an impact origin of preferred orientation in quartzite: an example from Vredefort, South Africa. Geology 33:273–276

Wooster WA, Wooster N (1946) Control of electrical twinning in quartz. Nature 157:405–406

Wooster WA, Wooster N, Rycroft JL, Thomas LA (1947) The control and elimination of electrical (Dauphiné) twinning in quartz. J Inst Electr Eng 94:927–938

Zinserling KV (1961) Artificial twinning of quartz (in Russian). Acad Sci USSR Moscow